Fiber-optic polarization diversity detection for rotary probe optical coherence tomography

Anthony M. D. Lee,[1] Hamid Pahlevaninezhad,[1] Victor X. D. Yang,[2] Stephen Lam,[1] Calum MacAulay,[1] and Pierre Lane[1,*]

[1]*Department of Integrative Oncology—Imaging Unit, British Columbia Cancer Agency Research Centre, Vancouver, British Columbia, Canada*

[2]*Biophotonics and Bioengineering Laboratory, Department of Electrical and Computer Engineering, Ryerson University, Toronto, Ontario, Canada*

**Corresponding author: plane@bccrc.ca*

Received April 2, 2014; revised May 7, 2014; accepted May 7, 2014; posted May 9, 2014 (Doc. ID 209407); published June 12, 2014

We report a polarization diversity detection scheme for optical coherence tomography with a new, custom, miniaturized fiber coupler with single mode (SM) fiber inputs and polarization maintaining (PM) fiber outputs. The SM fiber inputs obviate matching the optical lengths of the X and Y OCT polarization channels prior to interference and the PM fiber outputs ensure defined X and Y axes after interference. Advantages for this scheme include easier alignment, lower cost, and easier miniaturization compared to designs with free-space bulk optical components. We demonstrate the utility of the detection system to mitigate the effects of rapidly changing polarization states when imaging with rotating fiber optic probes in Intralipid suspension and during *in vivo* imaging of human airways.

OCIS codes: (110.4500) Optical coherence tomography; (060.2340) Fiber optics components; (120.1880) Detection; (170.0110) Imaging systems; (170.3890) Medical optics instrumentation.

http://dx.doi.org/10.1364/OL.39.003638

Medical applications for optical coherence tomography (OCT) imaging continue to expand [1] while the development of fiber optic OCT probes has allowed endoscopic imaging and intravascular use [2–8]. Rotary and rotary-pullback fiber optic probes are widely used scanning mechanisms for generating two-dimensional and three-dimensional OCT images, respectively, of cylindrically symmetric structures. These probes are commonly made using single mode (SM) optical fibers and driven from the proximal end using rotary motors with speedometer cables used to transmit the rotary motion to the distal imaging tip. As the spinning SM fiber is continuously flexing and in motion, the polarization state of the light being emitted from the tip is constantly varying. Mach–Zehnder OCT interferometers typically used for imaging have a fixed reference arm. Thus, interference between light from the nonmoving reference arm with fixed polarization state and the sample arm with varying polarization state introduced by the rotating probe causes artificial intensity variations during OCT imaging.

One approach to mitigating the polarization effects of only a rotating fiber optic sample arm is to use a common path probe where a partial reflection at the distal tip of the probe serves as the reference arm [9,10]. In this approach, both the sample and reference arms undergo the same polarization variations. However, being a Michelson OCT interferometer, this type of probe has less sensitivity relative to Mach–Zehnder interferometers [11]. An alternative approach to compensate for polarization effects in rotating probes is to use a polarization diversity detection (PDD) scheme [12–28]. In this scheme, polarization beam splitters (PBSs) are used following the sample/reference combiner to separate the interference signal into its orthogonal (X and Y) polarizations. The reference beam power is equalized between the two polarization states X and Y such that $E_{R,X} = E_{R,Y} = E_R$. In this way, variations in OCT image intensity can be eliminated by displaying the square root of the sum of the squares of the X and Y intensities.

PDD schemes have been realized in the literature using free-space optics configurations [14–20]. In this case, the X and Y orthogonal polarizations in the two arms following the 50/50 beam combiner are well defined with respect to each other. However, this type of setup is costly, difficult to miniaturize, and cumbersome since it involves the alignment of multiple beam splitters and collimators. Fiber-based PDD schemes are also reported using unbalanced receivers [21–24] and balanced receivers with 50/50 SM fiber couplers [25] and 50/50 polarization maintaining (PM) fiber couplers [26–28]. Systems with unbalanced receivers have less signal-to-noise ratio compared to systems with balanced receivers because of a lower detector dynamic range [11]. In addition, in PDD schemes with balanced 50/50 SM fiber couplers, the birefringence of the SM fiber outputs compromises well-defined orthogonal X and Y axes after interference. Furthermore, in PDD schemes with PM fiber couplers, the optical lengths of the coupler sample and reference input pigtails must be precisely matched to avoid different optical path lengths for the X and Y images because of PM fiber birefringence. There is also a commercially available fiber-based PDD scheme (PSOCT-1300, Thorlabs Inc.). However, balancing this setup requires iterative adjustment of up to four polarization controllers and does not necessarily converge rapidly to an acceptable solution.

In this Letter, we present a fiber-based PDD scheme that eliminates alignment issues encountered with free-space optical setups, is very simple to balance, and is relatively inexpensive. In this PDD scheme, a hybrid custom coupler with SM fiber inputs and PM fiber outputs combines the sample and reference arms, relieving the requirement for precise length matching prior to interference and with well-defined X and Y axes after interference. Using this scheme, we demonstrate the ability to

mitigate polarization artifacts in SM rotary probe OCT imaging in Intralipid suspension and in *in vivo* human airway imaging.

The swept-source OCT system used in this study is shown schematically in Fig. 1. Unless otherwise specified, all fiber optic components were purchased from AFW Technologies, Hallam, Australia. A 50.4 kHz swept source laser (SSOCT-1310, Axsun Technologies Inc., Billerica, Massachusetts) with 20 mW polarized output power centered at 1310 nm with 100 nm bandwidth (FWHM) is coupled 90% sample/10% reference into a single-mode Mach–Zehnder OCT interferometer. Polarization controllers (PLC-M02-NC-7, General Photonics, Chino, California) allow adjustment of the laser polarization prior to entry into sample and reference optical circulators. The sample arm consists of a fiber optic rotary joint (MJP-SAPB, Princetel Inc; Pennington, New Jersey) connected to a 0.9 mm diameter, rotationally driven, side-looking fiber optic probe (C7 Dragonfly Imaging Catheter, St. Jude Medical Inc, St. Paul, Minnesota). A custom built motor assembly allows rotational and pullback imaging capability.

A thin film polarizer (LPNIR050, Thorlabs Inc., Newton, New Jersey) mounted in a rotational mount is inserted before the reference arm end mirror to balance the reference polarization powers at the detectors as described below. This polarizer is mounted at an angle to prevent unwanted reflection artifacts.

Light returning from the sample and reference arms is combined using a specially designed 50/50 polarizing maintaining fiber coupler (PMFC) with SM fiber inputs and PM fiber outputs, shown in detail in the inset of Fig. 1. In this customized micro-optic coupler ordered from AFW Technologies, light entering ports R and S is collimated into beams by dual fiber collimators (DFC). Interference between these beams occurs at a nonpolarizing beam splitter (50/50 BS in the inset) that also splits the interference into two roughly equal intensity beams that subsequently get recoupled by DFCs to output ports 1 and 2. The PM fiber outputs are spliced to PBSs. Polarization matched outputs from the PBSs are connected to 75 MHz balanced detectors (PDB420C, Thorlabs Inc.) constituting the X and Y detection channels. $P_{S\to X1/X2/Y1/Y2} = 3.72/3.63/3.74/3.71$ dB and $P_{R\to X1/X2/Y1/Y2} = 4.07/3.98/3.75/3.71$ dB with ± 40 nm 3 dB bandwidth. The PMFC's SM fiber inputs obviate matching of the optical path lengths of the sample and reference input pigtails prior to interference at the PMFC. If a PM fiber is used on the PMFC inputs, the lengths of these two fiber segments must be matched to less than the beat length of the PM fiber (typically a few millimeters for a PANDA fiber at 1310 nm) or else the X and Y images will be shifted axially relative to each other. A PM fiber is required on the backside of the coupler to ensure defined X and Y axes. A high speed digitizer (ATS9350, Alazar Technologies Inc., Pointe-Claire, Quebec) in "k-clock" acquisition mode collects the data. Custom written data acquisition software provides real time 2D OCT imaging.

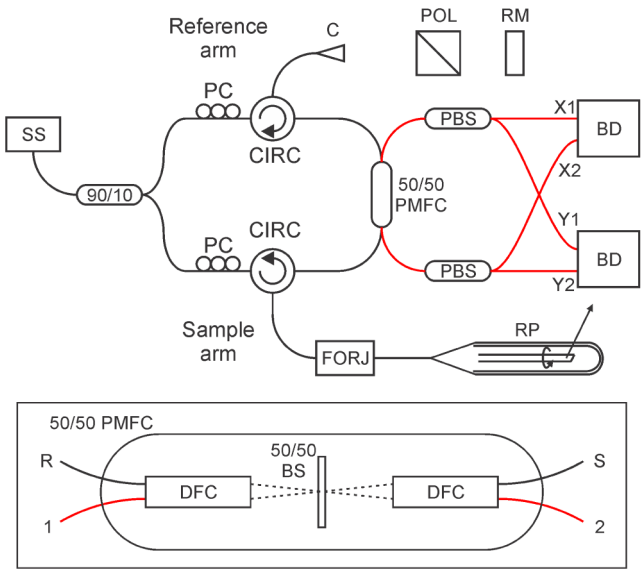

Fig. 1. Schematic diagram of endoscopic OCT system. SS, swept-source laser; PC, polarization controller; CIRC, circulator; C, collimator; POL, polarizer; RM, reference mirror; FORJ, fiber optic rotary joint; RP, rotary probe; PMFC, polarization maintaining fiber coupler; PBS, polarization beam splitter; BD, balanced detector. Red lines indicate PM fiber; all others are SM fiber. Inset: Internal schematic of the micro-optic 50/50 PMFC. DFC, dual fiber collimator; 50/50 BS, 50/50 polarization independent beam splitter. Internal light paths are denoted by dashed lines. Light entering either port R or S outputs to both ports 1 and 2.

Balancing of the reference arm's reflected power into the X and Y arms of the PDD setup is accomplished by minimizing the quantity $(S_{X1} + S_{X2} - S_{Y1} - S_{Y2})$ by adjusting the orientation of the reference arm polarizer, where S_i are the four slow monitor outputs on the balanced detectors. This is easily accomplished using a multichannel oscilloscope with on-board math functions. Because of the spectral variation of the optical components, it is impossible to completely balance the two detection channels over the entire laser sweep. An acceptable compromise, however, can be made by minimizing the integral of the detector signals over the entire laser sweep.

At this point, the PDD setup is balanced but the total power throughput of the reference arm may be reduced because of rejection by the polarizer. The power throughput by the reference arm may be increased by adjusting the polarization controller preceding the reference arm. Because of the spectral variation of the components along the reference arm through to the detectors, the PDD setup may become slightly unbalanced after power optimization. In this case, small adjustments of the polarizer can again restore X and Y balancing. Further, readjustment of the polarizer and polarization controller is typically not required but can be performed if deemed necessary. It should be noted that if light entering the reference arm is polarized, the polarizer can be replaced by a quarter-wave plate or half-wave plate. The use of a wave plate reduces reference arm losses compared to that with the polarizer and obviates the need for reference arm polarization controller adjustment.

Taking E_S and E_R as the optical electric fields returning from the sample and reference arms at the input ports of the PMFC, respectively, the PMFC output electric fields are:

$$\vec{E}_1 = \frac{1}{\sqrt{2}}(\vec{E}_S + i\vec{E}_R), \quad (1)$$

$$\vec{E}_2 = \frac{1}{\sqrt{2}}(i\vec{E}_S + \vec{E}_R). \quad (2)$$

The PBSs separate the X and Y components of the PMFC outputs, resulting in the following optical electric fields at the detector inputs:

$$\begin{aligned} E_{X1} &= \frac{1}{\sqrt{2}}(E_S\cos(\theta_S) + iE_R),\\ E_{X2} &= \frac{1}{\sqrt{2}}(iE_S\cos(\theta_S) + E_R),\\ E_{Y1} &= \frac{1}{\sqrt{2}}(E_S\sin(\theta_S) + iE_R),\\ E_{Y2} &= \frac{1}{\sqrt{2}}(iE_S\sin(\theta_S) + E_R), \end{aligned} \quad (3)$$

where $\vec{E}_S = E_S\cos(\theta_S)\hat{x} + E_S\sin(\theta_S)\hat{y}$ and the balancing procedure ensures that $E_{R,X} = E_{R,Y} = E_R$. Variations in the sample arm polarization due to the rotating fiber change θ_S. Using balanced detection ($I_X = I_{X1} - I_{X2}$ and $I_Y = I_{Y1} - I_{Y2}$), the electrical signals measured for I_X and I_Y are proportional to $\cos(\theta_S)$ and $\sin(\theta_S)$, respectively. Thus, the quantity

$$I_{XY} = \sqrt{I_X^2 + I_Y^2} \quad (4)$$

is independent of θ_S, providing OCT structural images with suppressed polarization artifacts.

Figure 2 shows an image of a 1% Intralipid suspension obtained using the rotary probe. Since the suspension is isotropic, the image should have no variation with respect to the azimuthal coordinate. The images generated from the individual polarization channels X and Y, shown in Figs. 2(a) and 2(b), respectively, clearly show the effects of varying polarization from the rotating probe that cause variations in intensity with respect to the azimuthal coordinate. In the polarization insensitive image generated using Eq. (4) and shown in Fig. 2(c), the variation of the intensity with respect to the azimuthal coordinate is clearly much reduced. Plotted in Fig. 2(d) are the intensities of the intralipid images in Figs. 2(a)–2(c) averaged along the axial dimension versus the azimuthal coordinate, again displaying the suppression of the polarization artifacts. For the frame in Fig. 2, the standard deviations of the axially integrated X and Y images over the azimuthal coordinate are 0.48 and 0.54, respectively, much larger than that of the polarization insensitive image (0.14). Thus, our PDD scheme reduces the image polarization variations by a factor greater than three.

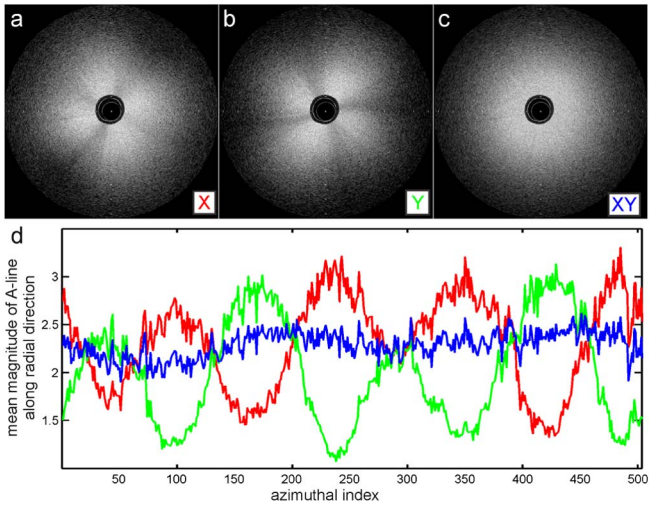

Fig. 2. (a), (b) Polarization diverse and (c) polarization insensitive images of 1% Intralipid suspension. (d) Plots of the averages of the A-lines taken along the radial direction for the images shown in (a)–(c).

The fiber PDD scheme was also used for *in vivo* lung imaging. In this situation, an additional closed ended sheath was used over the open-ended probe to prevent direct probe-patient contact. A bronchoscope was used to guide the OCT probe to the imaged airway. *In vivo* human lung imaging was approved by the Research Ethics Board of the University of British Columbia and the British Columbia Cancer Agency. The subject gave written, informed consent. An image frame of *in vivo* human lung is shown in Fig. 3. Figures 3(a) and 3(b) show the X and Y channels, respectively. Corresponding red and green arrows indicate regions where there is intensity trading between the two channels because of varying polarization emitted from the rotary probe. The polarization insensitive image, presented in Fig. 3(c), clearly shows that PDD improves the ability to discern tissue morphology.

Using current pricing, this fiber optic PDD implementation costs approximately a third of the price of an analogous PDD scheme made with bulk optical components and mounts from a major optomechanical parts supplier. Reduced cost, ease of use, and compactness are key advantages of this PDD scheme for commercial OCT systems. This PDD scheme is also useful for polarization sensitive OCT (PSOCT) imaging systems where similar advantages should be realized. We explore this application in a following paper [29]. With the explosion of OCT imaging systems designed for endoscopic use in a variety of body sites, we expect this PDD scheme to be well received by the OCT imaging community.

In conclusion, we present a new polarization diversity detection scheme for OCT built around a fiber-based

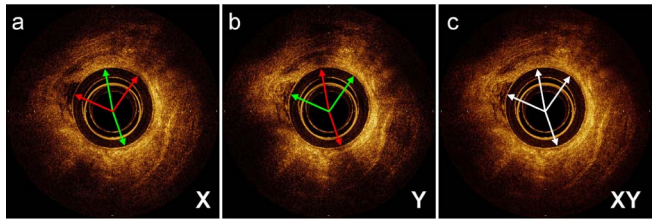

Fig. 3. (a), (b) Polarization diverse and (c) polarization insensitive images of *in vivo* human airway. Arrows indicate large positive (green) and negative (red) intensity variations in the X and Y images because of fluctuating polarization emitted from the rotating probe.

polarization maintaining fiber coupler and fiber-optic polarization beam splitters. We demonstrate that this cost-effective, easy to build, and easy to balance PDD scheme effectively mitigates polarization effects when using SM rotary fiber optic OCT probes.

References

1. B. E. Bouma, S. H. Yun, B. J. Vakoc, M. J. Suter, and G. J. Tearney, Curr. Opin. Biotechnol. **20**, 111 (2009).
2. G. J. Tearney, S. A. Boppart, B. E. Bouma, M. E. Brezinski, N. J. Weissman, J. F. Southern, and J. G. Fujimoto, Opt. Lett. **21**, 543 (1996).
3. J. G. Fujimoto, S. A. Boppart, G. J. Tearney, B. E. Bouma, C. Pitris, and M. E. Brezinski, Heart **82**, 128 (1999).
4. X. Li, C. Chudoba, T. Ko, C. Pitris, and J. G. Fujimoto, Opt. Lett. **25**, 1520 (2000).
5. X. D. Li, S. A. Boppart, J. van Dam, H. Mashimo, M. Multinga, W. Drexler, M. Klein, C. Pitris, M. L. Krinsky, M. E. Brezinski, and J. G. Fujimoto, Endoscopy **32**, 921 (2000).
6. X. Li, T. H. Ko, and J. G. Fujimoto, Opt. Lett. **26**, 1906 (2001).
7. G. T. Bonnema, K. Cardinal, S. K. Williams, and J. K. Barton, J. Biophoton. **2**, 353 (2009).
8. D. Lorenser, X. Yang, R. W. Kirk, B. C. Quirk, R. A. McLaughlin, and D. D. Sampson, Opt. Lett. **36**, 3894 (2011).
9. A. R. Tumlinson, J. K. Barton, B. Považay, H. Sattman, A. Unterhuber, R. A. Leitgeb, and W. Drexler, Opt. Express **14**, 1878 (2006).
10. J. U. Kang, J. Han, and K. Zhang, J. Opt. Soc. Korea **14**, 1 (2010).
11. A. M. Rollins and J. A. Izatt, Opt. Lett. **24**, 1484 (1999).
12. M. Kobayashi, H. Hanafusa, K. Takada, and J. Noda, J. Lightwave Technol. **9**, 623 (1991).
13. B. L. Heffner and W. V. Sorin, "Polarization independent optical coherence-domain reflectometry," U. S. patent 5,202,745A (April 13, 1993).
14. W. Y. Oh, S. H. Yun, B. J. Vakoc, M. Shishkov, A. E. Desjardins, B. H. Park, J. F. de Boer, G. J. Tearney, and B. E. Bouma, Opt. Express **16**, 1096 (2008).
15. K. H. Kim, B. H. Park, Y. Tu, T. Hasan, B. Lee, J. Li, and J. F. de Boer, Opt. Express **19**, 552 (2011).
16. B. Baumann, W. Choi, B. Potsaid, D. Huang, J. S. Duker, and J. G. Fujimoto, Opt. Express **20**, 10218 (2011).
17. Z. Li, D. K. Kasaragod, and S. J. Matcher, Phys. Med. Biol. **56**, 1105 (2011).
18. E. Z. Zhang, W. Y. Oh, M. L. Villiger, L. Chen, B. E. Bouma, and J. Vakoc, Opt. Express **21**, 1163 (2013).
19. M. Villinger, E. Z. Zhang, S. K. Nadkarni, W. Y. Oh, B. J. Vakoc, and B. E. Bouma, Opt. Express **21**, 16353 (2013).
20. M. J. Ju, Y. J. Hong, S. Makita, Y. Lim, K. Kurokawa, L. Duan, M. Miura, S. Tang, and Y. Yasuno, Opt. Express **21**, 19412 (2013).
21. M. C. Pierce, B. H. Park, B. Cense, and J. F. de Boer, Opt. Lett. **27**, 1534 (2002).
22. B. H. Park, M. C. Pierce, B. Cense, and J. F. de Boer, Opt. Express **11**, 782 (2003).
23. B. H. Park, M. C. Pierce, B. Cense, and J. F. de Boer, Opt. Lett. **29**, 2512 (2004).
24. M. C. Pierce, M. Shishkov, B. H. Park, N. A. Nassif, B. E. Bouma, G. J. Tearney, and J. F. de Boer, Opt. Express **13**, 5739 (2005).
25. S. H. Yun, G. J. Tearney, B. J. Vadoc, M. Shishkov, W. Y. Oh, A. E. Desjardins, M. J. Suter, R. C. Chan, J. A. Evans, I. K. Jang, N. S. Nishioka, J. F. de Boer, and B. E. Bouma, Nat. Med. **12**, 1429 (2006).
26. M. Yamanari, S. Makita, and Y. Yasuno, Opt. Express **16**, 5892 (2008).
27. M. Bonesi, H. Sattmann, T. Torizicky, S. Zotter, B. Baumann, M. Pircher, E. Götzinger, C. Eigenwillig, W. Wieser, R. Huber, and C. K. Hitzenberger, Biomed. Opt. Express **3**, 2987 (2012).
28. Z. Lu, D. Kasaragod, and S. J. Matcher, Opt. Express **5**, 763 (2014).
29. H. Pahlevaninezhad, A. M. D. Lee, S. Lam, C. MacAulay, and P. M. Lane, "A fiber-based polarization-sensitive optical coherence tomography system with fiber-based passive components," Opt. Express (submitted).